KA-THEP-5-1995
March 1995

Z BOSON OBSERVABLES IN THE MSSM*

A. DABELSTEIN† , W. HOLLIK, W. MÖSLE†

Institut für Theoretische Physik, Universität Karlsruhe, Kaiserstr. 12
D-76128 Karlsruhe, Germany
E-mail: add@dmumpiwh.bitnet

ABSTRACT

A combined analysis for Z boson observables and the quantity Δr within the framework of the Minimal Supersymmetric Standard Model is presented. Contributions from supersymmetric particles are discussed and upper and lower bounds for the MSSM predictions are given.

1. Introduction

Precision data at LEP have reached a level of accuracy where the electroweak theory can be tested at its quantum structure. The predictions of the Standard Model for the precision observables at the Z resonance have been calculated with full one-loop and leading higher order contributions[1,2]. With two exceptions, all precision observables, measured at the level of a few per mille or even better, agree with the Standard Model predictions within 1σ [3]. The top quark mass $m_t = 180 \pm 12$ GeV as the weighted average of the CDF and DØ measurements[4] is in good agreement with the Standard Model implication from the precision data. The only mismatch is found in the ratios of the hadronic partial decay widths $Z \to c\bar{c}\,(b\bar{b})$ to the total hadronic width :

$$R_c = \frac{\Gamma_c}{\Gamma_{had}} \ , \ R_b = \frac{\Gamma_b}{\Gamma_{had}} \ ,$$

which deviate by $\approx 2\sigma$ from the recent LEP data[3].

It is not unlikely that the Standard Model around the Z scale is the effective low energy limit of a more comprehensive theory of the GUT class. Within these ideas the extension of the Standard Model to the Minimal Supersymmetric Standard Model (MSSM)[5] is of particular theoretical interest, allowing the unification of gauge couplings at the GUT scale $\mathcal{O}(10^{15}$ GeV)[6].

At present the MSSM is the most predictive framework for physics beyond the Standard Model. The superpartners appear in the electroweak radiative corrections

* To appear in the Proceedings of the Ringberg Workshop "Perspectives for Electroweak Interactions in e^+ e^- Collisions", February 5-8, 1995.
†E-Mail: add@dmumpiwh.bitnet, wom@dmumpiwh.bitnet

and thus enter the theoretical predictions for the precision observables with the property that they decouple in the heavy mass limit. Precision measurements therefore provide a tool for indirect tests of the MSSM and for probing the possible mass range of new particles beyond the present limits from negative direct searches.

As an extension of the Standard Model, the general 2-Higgs doublet has been discussed for Z boson decays[7] and implications from electroweak precision data are presented in ref.[8], also for a supersymmetric Higgs sector under the assumption of decoupling genuine SUSY particles. Recently, supersymmetric contributions for individual Z boson decay widths and ratios R_b, R_c were presented in refs[9,10,11,12,13].

In this article we describe the results of a complete MSSM 1-loop calculation for a combined discussion of all Z observables and M_W. The Z boson observables together with the quantity Δr (or M_W) depend sizeably on the masses and parameters of the virtual standard and supersymmetric particles. For each observable the effects from the parameters in the various relevant MSSM sectors are discussed and comparisons with the minimal Standard Model are performed. Considering the Z boson observables and Δr globally as functions of the MSSM parameter set, the following conclusions can be observed:

- the MSSM can improve the agreement of the individually predicted observables with the experimental data. It is, however, difficult to remove the discrepancies from all observables simultaneously.

- a χ^2 fit for all input parameters gives a prefered set of MSSM parameters. This numerical analysis yields constraints on the supersymmetric particle masses and parameters. A prediction for a supersymmetric particle spectrum can not be achieved without additional assumptions, since the precision observables are only weakly sensitive to equal supersymmetric masses ≥ 500 GeV[14].

In the following, the considered Z boson observables and their notation are introduced. A brief description of the one-loop and higher order corrections of the precision observables is presented and the parametrization of the MSSM is given. The discussion compares the MSSM predictions with the experimental data and presents constraints on the supersymmetric parameter space.

2. Z^0 boson on-resonance observables

At the Z boson resonance two classes of precision observables are available:

a) inclusive quantities:

- the partial leptonic and hadronic decay width $\Gamma_{f\bar{f}}$,
- the total decay width Γ_Z,

- the hadronic peak cross section σ_h,
- the ratio of the hadronic to the electronic decay width of the Z boson: R_h,
- the ratio of the partial decay width for $Z \to c\bar{c}\,(b\bar{b})$ to the hadronic width, R_c, R_b.

b) asymmetries and the corresponding mixing angles:

- the *forward-backward* asymmetries A_{FB}^f,
- the *left-right* asymmetries A_{LR}^f,
- the τ polarization P_τ,
- the effective weak mixing angles $\sin^2\theta_{eff}^f$.

Together with the quantity Δr in the correlation of the W mass to the electroweak input parameters G_μ, M_Z and α_{EM}, this set of precision observables is convenient for a numerical analysis of the supersymmetric parameter space.

2.1. The effective Z-f-f couplings

The coupling of the Z boson to fermions f can be expressed by effective vector and axial vector coupling constants v_{eff}^f, a_{eff}^f in terms of the NC vertex:

$$J_{NC}^\mu = \frac{e}{2s_W^2 c_W^2}\,\gamma^\mu\,(v_{eff}^f - a_{eff}^f\gamma_5)\ , \tag{1}$$

where the convention is introduced : $c_W^2 = \cos^2\theta_W = 1 - s_W^2 = M_W^2/M_Z^2$ [15]. Input parameters are the μ decay constant $G_\mu = 1.166392 \times 10^{-5}$ GeV^{-2}, $\alpha_{EM} = 1/137.036$ and the mass of the Z^0 boson $M_Z = 91.1887$ GeV. The mass of the W boson is related to these input parameters through:

$$\frac{G_\mu}{\sqrt{2}} = \frac{\pi\alpha_{EM}}{2s_W^2 M_W^2}\cdot\frac{1}{1-\Delta r_{MSSM}\,(\alpha_{EM}, M_W, M_Z, m_t, ...)}\ , \tag{2}$$

where the complete MSSM one-loop contributions are parametrized by the quantity Δr_{MSSM}[16]. Leading higher order Standard Model corrections[1,17] to the quantity Δr are included in the calculation.

The effective couplings v_{eff}^f, a_{eff}^f can be written as:

$$\begin{aligned} v_{eff}^f &= \sqrt{Z_Z}\,(v^f + \Delta v^f + Z_M Q_f) \\ a_{eff}^f &= \sqrt{Z_Z}\,(a^f + \Delta a^f)\ . \end{aligned} \tag{3}$$

v^f and a^f are the tree-level vector and axial vector couplings:

$$v^f = I_3^f - 2Q_f s_W^2\ ,\ a^f = I_3^f. \tag{4}$$

Z_Z, Z_M are given in Eq. (9). The complete MSSM one-loop contributions of the non-universal finite vector and axial vector couplings Δv^f, Δa^f have been calculated[14], together with the leading two-loop Standard Model contributions[1,2]. They are derived in the 't Hooft-Feynman gauge and in the on-shell renormalization scheme[18].

The universal finite Z boson wave function renormalization Z_Z and the γZ mixing Z_M are derived from the (γ, Z) propagator matrix. The inverse matrix is:

$$(\Delta_{\mu\nu})^{-1} = ig_{\mu\nu} \begin{pmatrix} k^2 + \hat{\Sigma}_\gamma(k^2) & \hat{\Sigma}_{\gamma Z}(k^2) \\ \hat{\Sigma}_{\gamma Z}(k^2) & k^2 - M_Z^2 + \hat{\Sigma}_Z(k^2) \end{pmatrix} , \tag{5}$$

where $\hat{\Sigma}_\gamma$, $\hat{\Sigma}_Z$, $\hat{\Sigma}_{\gamma Z}$ are the renormalized self energies and mixing. They are obtained by summing the loop diagrams and the counter terms[1].

The entries in the (γ, Z) propagator matrix:

$$\Delta_{\mu\nu} = -ig_{\mu\nu} \begin{pmatrix} \Delta_\gamma & \Delta_{\gamma Z} \\ \Delta_{\gamma Z} & \Delta_Z \end{pmatrix} , \tag{6}$$

are given by:

$$\begin{aligned} \Delta_\gamma(k^2) &= \frac{1}{k^2 + \hat{\Sigma}_\gamma(k^2) - \frac{\hat{\Sigma}^2_{\gamma Z}(k^2)}{k^2 - M_Z^2 + \hat{\Sigma}_Z(k^2)}} \\ \Delta_Z(k^2) &= \frac{1}{k^2 - M_Z^2 + \hat{\Sigma}_Z(k^2) - \frac{\hat{\Sigma}^2_{\gamma Z}(k^2)}{k^2 + \hat{\Sigma}_\gamma(k^2)}} \\ \Delta_{\gamma Z}(k^2) &= -\frac{\hat{\Sigma}_{\gamma Z}(k^2)}{[k^2 + \hat{\Sigma}_\gamma(k^2)]\,[k^2 - M_Z^2 + \hat{\Sigma}_Z(k^2)] - \hat{\Sigma}^2_{\gamma Z}(k^2)} . \end{aligned} \tag{7}$$

The renormalization condition to define the mass of the Z boson is given by the pole of the propagator matrix Eq. (5). The pole $k^2 = M_Z^2$ is the solution of the equation:

$$\mathcal{R}\mathrm{e}\,[\,(\mathrm{M}_\mathrm{Z}^2 + \hat{\Sigma}_\gamma(\mathrm{M}_\mathrm{Z}^2)\,)\,\hat{\Sigma}_\mathrm{Z}(\mathrm{k}^2) - \hat{\Sigma}^2_{\gamma\mathrm{Z}}(\mathrm{M}_\mathrm{Z}^2)\,] = 0 . \tag{8}$$

Eq. (7) yields the wave function renormalization Z_Z and mixing Z_M:

$$\begin{aligned} Z_Z &= Res_{M_Z}\Delta_Z = \left. \frac{1}{1 + \hat{\Sigma}'_Z(k^2) - \left(\frac{\hat{\Sigma}^2_{\gamma Z}(k^2)}{k^2 + \hat{\Sigma}_\gamma(k^2)}\right)} \right|_{k^2 = M_Z^2} \\ Z_M &= -\frac{\hat{\Sigma}_{\gamma Z}(M_Z^2)}{M_Z^2 + \hat{\Sigma}_\gamma(M_Z^2)} . \end{aligned} \tag{9}$$

2.2. Z boson observables

The fermionic Z boson partial decay widths $\Gamma_{f\bar{f}}$ can be written:

1) $f \neq b$:

$$\Gamma_{f\bar{f}} = \frac{N_C\,\alpha_{EM}\,M_Z}{3}\sqrt{1-\frac{4m_f^2}{M_Z^2}}\left[(v_{eff}^f)^2(1+\frac{2m_f^2}{M_Z^2})+(a_{eff}^f)^2(1-\frac{4m_f^2}{M_Z^2})\right]\cdot$$
$$\cdot(1+\frac{3\alpha_{EM}}{4\pi}Q_f^2)\,(1+\delta_{QCD}^f)\ , \tag{10}$$

where

$$\delta_{QCD}^f = \begin{cases} 0 & ,f=\text{leptons} \\ \frac{\alpha_s}{\pi}+1.405(\frac{\alpha_s}{\pi})^2-12.8(\frac{\alpha_s}{\pi})^3 & ,f=\text{quarks} \end{cases}\ . \tag{11}$$

2) $f = b$:

$$\Gamma_{b\bar{b}} = \alpha_{EM}\,M_Z\left[(v_{eff}^b)^2+(a_{eff}^b)^2\right]\cdot(1+\frac{3\alpha_{EM}}{4\pi}Q_b^2)\,(1+\delta_{QCD}^b)+\Delta\Gamma_{b\bar{b}}\ . \tag{12}$$

In $\Delta\Gamma_{b\bar{b}}$ the b quark specific finite mass terms and QCD corrections together with the leading two-loop $\mathcal{O}(\alpha_{\rm EM}\alpha_{\rm S})$ are included[1,2]. δ_{QCD}^b is given in Eq. (11).

The total decay width Γ_Z is the sum of the leptons and quarks:

$$\Gamma_Z = \sum_f \Gamma_{f\bar{f}}\ . \tag{13}$$

In the following $\Gamma_{had} = \sum_q \Gamma_{q\bar{q}}$ is the hadronic decay width of the Z boson.

The hadronic peak cross section:

$$\sigma_h = \frac{12\pi}{M_Z^2}\frac{\Gamma_{ee}\Gamma_{had}}{\Gamma_Z^2}\ . \tag{14}$$

The ratio of the hadronic to the electronic decay width is defined:

$$R_e = \frac{\Gamma_{had}}{\Gamma_{ee}}\ . \tag{15}$$

The ratio of the partial decay width for $Z \to b\bar{b}\,(c\bar{c})$ to the total hadronic decay width:

$$R_{b(c)} = \frac{\Gamma_{b\bar{b}(c\bar{c})}}{\Gamma_{had}}\ . \tag{16}$$

The following quantities and observables depend on the ratio of the vector to the axial vector coupling. The effective flavour dependent weak mixing angle can be written:

$$\sin^2\theta_{eff}^f = \frac{1}{4|Q_f|}\left(1-\frac{v_{eff}^f}{a_{eff}^f}\right)\ . \tag{17}$$

Table 1: Experimental LEP and $p\bar{p}$ results.

Γ_Z [GeV]	2.4971	$\pm$	0.0032
σ_h [GeV]	41.492	$\pm$	0.081
R_e	20.843	$\pm$	0.060
R_μ	20.805	$\pm$	0.048
R_τ	20.798	$\pm$	0.066
A_{FB}^e	0.0154	$\pm$	0.0030
A_{FB}^μ	0.0160	$\pm$	0.0017
A_{FB}^τ	0.0209	$\pm$	0.0024
R_b	0.2204	$\pm$	0.0020
R_c	0.1606	$\pm$	0.0095
A_{FB}^b	0.1015	$\pm$	0.0036
A_{FB}^c	0.0760	$\pm$	0.0089
Δr	0.0425	$\pm$	0.009

The *left-right* asymmetries:

$$A_{LR}^f = \mathcal{A}^{\rm f} = \frac{2\, v_{eff}^f / a_{eff}^f}{1 + (v_{eff}^f / a_{eff}^f)^2} \ . \tag{18}$$

The *forward-backward* asymmetries:

$$A_{FB}^f = \frac{3}{4}\, \mathcal{A}^{\rm e}\, \mathcal{A}^{\rm f} \ . \tag{19}$$

3. Discussion

The experimental results from the recent LEP and $p\bar{p}$ data are summarized in table 1[3,19]. In addition to the measurements, the correlation matrix[3] is used. The value for $\alpha_S(M_Z^2)$ has been fixed from QCD observables at the Z pole[20]:

$$\alpha_S(M_Z^2) = 0.123 \pm 0.006 \ , \tag{20}$$

and the b quark mass $m_b = 4.7$ GeV. In the following we discuss the general version of the MSSM without further restrictions to the parameters from assumptions about Grand Unification or Supergravity.

3.1. Higgs sector

The Higgs sector of the MSSM is that of a two Higgs doublet model, where the coefficients of the potential are restricted by supersymmetry. As a consequence of the

supersymmetric Higgs potential, a light Higgs boson exists with a tree level upper mass bound given by the Z boson mass. The Higgs potential contains two independent free parameters, which are $\tan\beta = v_2/v_1$ and the mass of the pseudoscalar Higgs boson M_{A^0}. v_1, v_2 are the vacuum expectation values of the Higgs doublets.

Radiative corrections to the Higgs mass spectrum predict an upper limit of the light Higgs mass $\mathcal{O}(130\ \mathrm{GeV})$[21]. In the calculation of the neutral scalar MSSM Higgs mass spectrum and the mixing angle α the corrections $\mathcal{O}(\mathrm{m_t^4})$ are included[22].

Fig. 1 shows the dependence of a subset of observables: Δr, R_b, R_c, $R_h = R_e$, Γ_{tot}, Γ_{ee}, $\sin^2\theta^e_{eff}$, A^b_{FB} and A^c_{FB} as functions on M_A for values $\tan\beta = 0.7$ (dotted), 1.5 (long dotted), 8 (dashed-dotted), 20 (dashed), 70 (solid). This set of observables is convenient for a qualitative discussion of the universal and non-universal MSSM one-loop contributions. The top quark mass is fixed at $m_t = 174$ GeV, and squark, slepton masses are $m_{\tilde{q}} = 500$ GeV, $m_{\tilde{l}} = 800$ GeV without left-right mixing. The soft breaking parameters in the gaugino sector are $\mu = 100$ GeV, $M = 300$ GeV and a heavy gluino mass $m_{\tilde{gl}} = 800$ GeV is fixed. This set of genuine supersymmetric masses does not show sizeable effects on these observables and allows to explore only the SUSY Higgs sector.

A complete discussion on the quantity Δr (δM_W) is available[16], however, the inclusion of $\mathcal{O}(\mathrm{m_t^4})$ Higgs mass and $\mathcal{O}(\alpha_{\mathrm{EM}}\alpha_{\mathrm{S}}^2)$ contributions[22,1] improve the theoretical Δr predictions. In Fig. 1 the quantity Δr increases with M_A and is almost constant above $M_A \geq 250$ GeV. Small $\tan\beta = 0.7$ values give sizeable positive contributions to Δr, since radiative corrections to the scalar Higgs mass are large in the regime of small $M_A < 100$ GeV and small $\tan\beta$. In the mass range $M_A < 70$ GeV and $\tan\beta \geq 2$ the quantity Δr decreases and disfavours with the experimental data within the range of the measured top quark mass. Contributions of genuine supersymmetric masses (next subsection) do not increase Δr and enhance the deviation from the experimental result even stronger. A similar conclusion for the parameters M_A, $\tan\beta$ is obtained in Fig. 1 for the quantity $\sin^2\theta^e_{eff}$.

In the $\tan\beta < 1$ range the ratio R_b decreases for values $M_A < 500$ GeV. This effect is strong for small $M_A \approx 50$ GeV and yields the Standard Model results for $M_A \to \infty$. For intermediate $\tan\beta$, $4 < \tan\beta < 30$, R_b is nearly constant for 50 GeV $\leq M_A \leq 500$ GeV and agrees with the Standard Model prediction. Large $\tan\beta \approx 70$ enhance R_b for small $M_A \leq 55$ GeV, within the experimental 1σ bounds. In Fig. 1 this peak at $M_A = 46$ GeV is shown, however this scenario would predict a rather light neutral Higgs mass M_{h^0}. For $M_A \geq 75$ GeV the ratio R_b decreases, reaches a minimum for $M_A = 150$ GeV and approaches the SM result for larger pseudoscalar masses. The ratio R_c in Fig. 1 lies above the experimental 1σ bounds. Recently, the complementary $R_b - R_c$ effects have also been discussed[11]. However, the R_c sensitivity on the Higgs sector is small and only for large $\tan\beta = 70$ and 40 GeV $< M_A <$ 60 GeV the agreement with the experimental data is improved.

The total decay width Γ_{tot} and the ratio R_h in Fig. 1 show a qualitatively similar line shape as the ratio R_b. Γ_{tot} and R_h depend strongly on α_s, however, the "peak" region in R_b for $M_A < 70$ GeV and small (large) $\tan\beta < 1 (> 40)$ yields values for the quantities Γ_{tot}, R_h which are larger than the experimental results. A better agreement can be obtained by decreasing the total value of α_s.

3.2. Sfermion and Gaugino/Higgsino sector

Sfermions and charginos (neutralinos) appear in the vertex correction to Z boson decays and give sizeable contributions for the external b state. The chargino (neutralino) masses and the mixing angles in the gaugino couplings are calculated from soft breaking parameters M, M' and μ in the chargino (neutralino) mass matrix[5]. The validity of the GUT relation $M' = 5/3 \tan\theta_W M$ is assumed.

Squarks and sleptons are described by a 2×2 mass matrix:

$$\mathcal{M}^2_{\tilde{\mathrm{f}}} = \begin{pmatrix} M^2_{\tilde{Q}} + m^2_f + M^2_Z(I^f_3 - Q_f s^2_W)\cos 2\beta & m_f(A_f + \mu\{\cot\beta, \tan\beta\}) \\ m_f(A_f + \mu\{\cot\beta, \tan\beta\}) & M^2_{\{\tilde{U},\tilde{D}\}} + m^2_f + M^2_Z Q_f s^2_W \cos 2\beta \end{pmatrix} , \tag{21}$$

with SUSY soft breaking parameters $M_{\tilde{Q}}$, $M_{\tilde{U}}$, $M_{\tilde{D}}$, A_f, and μ. The notation in the off-diagonal entries in Eq. (21):

$$A'_f = A_f + \mu\{\cot\beta, \tan\beta\} , \tag{22}$$

will be used. Up and down type sferminos in (21) are distinguished by setting f=u,d and the $\{u, d\}$ entries in the parenthesis. Instead of $M_{\tilde{Q}}$, $M_{\tilde{U}}$, $M_{\tilde{D}}$, A'_b, A'_t, the physical squark masses are given by $m_{\tilde{b}} = m_{\tilde{b}_L} = m_{\tilde{b}_R}$, $m_{\tilde{t}_2}$ and A'_t. No left-right mixing for $\tilde{b}$ squarks is assumed and the $\tilde{u}$, $\tilde{d}$, $\tilde{c}$, $\tilde{s}$ masses are equal to the $\tilde{b}$ squark mass. The sneutrino masses $m_{\tilde{\nu}}$ are given without left-right mixing for sleptons.

In Fig. 2 the dependence of the Z boson observables and Δr for sbottom masses $m_{\tilde{b}} = 150\,(500)$ GeV, and stop masses $m_{\tilde{t}_R} = 50$ GeV (solid line), 150 GeV (dotted, dotted-dashed), 300 (500) GeV (long dotted, dashed) is shown as a function of $\tan\beta$. No left-right mixing in the stop states is assumed. $m_t = 174$ GeV, $\mu = 100$ GeV, $M = 100$ GeV, $M_A = 800$ GeV, $m_{\tilde{l}} = 900$ GeV and $m_{\tilde{g}l} = 900$ GeV.

Sfermion and chargino (neutralino) contributions decrease the quantity Δr[16]. Charginos and neutralinos give numerically small effects, large $\tilde{u}_L$-$\tilde{d}_L$ mass splittings in the squark and slepton sector are the dominant supersymmetric contributions. The quantity Δr gets sizeable contributions from the ρ parameter:

$$\Delta r \simeq \Delta\alpha_{EM} - \frac{c^2_W}{s^2_W}\Delta\rho + \ldots . \tag{23}$$

The $\tilde{b}_L$-$\tilde{t}_L$ mass splitting is described by the $\Delta\rho$ parameter[16]:

$$\Delta\rho^0_{\tilde{b}-\tilde{t}} = \frac{3\alpha_{EM}}{16\pi s^2_W M^2_W}\left(m^2_{\tilde{b}_L} + m^2_{\tilde{t}_L} - 2\frac{m^2_{\tilde{b}_L} m^2_{\tilde{t}_L}}{m^2_{\tilde{b}_L} - m^2_{\tilde{t}_L}} \log\frac{m^2_{\tilde{b}_L}}{m^2_{\tilde{t}_L}}\right) , \tag{24}$$

and decreases Δr for light $\tilde{b}$ masses[a]. Fig. 2 shows Δr for sbottom masses $m_{\tilde{b}} = 150\,(500)$ GeV, where a light $\tilde{b}$ mass decreases Δr sizeably. A variation in the stop state masses $m_{\tilde{t}_R}$ in Fig. 2 shows small contributions on Δr. The effect on left-right sfermion mixing is discussed in Fig. 3.

An enhancement of the ratio R_b can be observed for light charginos $\mathcal{O}(100$ GeV) and light stop-sbottom masses. This effect is stronger for small (large) $\tan\beta < 1 (> 40)$ values due to the $\tan\beta$ enhanced Yukawa type chargino (neutralino) - quark - squark couplings. Taking the present experimental limits on the genuine supersymmetric and Higgs masses into account, R_b can not be increased within the experimental 1σ bound. The enhancement in R_b is larger for light $\tilde{t}_R$ masses in Fig. 2, whereas R_b is nearly insensitive to the sbottom mass and therefore the $\tilde{t}_L$ mass.

The ratio R_h and the total decay width Γ_{tot} increase for light left or right sfermion states in Fig. 2. For $m_t = 174$ GeV and $\alpha_s = 0.123$, a light $\tilde{b}$ squark $m_{\tilde{b}} = 150$ GeV increases Γ_{tot} by about 2σ above the present experimental data. This enhancement for light sbottom masses is shown for the electronic decay width Γ_{ee}, where no sensitivity for $\tilde{t}_R$ masses can be observered. The *forward-backward* asymmetry A^b_{FB} also favours larger sbottom masses and shows smaller effects from $m_{\tilde{t}_R}$. Light $\tilde{b}_L$ masses increase the *forward-backward* asymmetries A^b_{FB}, A^c_{FB}.

Sfermion mixing for the parameter set in Fig. 2 "screens" the contributions from supersymmetric particles for all displayed observables. In Fig. 3, $m_{\tilde{b}} = 150$ GeV, $m_{\tilde{t}_2} = 50$ GeV and all other parameters are as in Fig. 2. The stop mixing is shown for $A'_t = -930$ GeV (dotted-dashed), -464 GeV (dashed), 0 (solid), 464 GeV (dotted), 930 GeV (long dotted). These A'_t mixing values yield $\tilde{t}_1$ masses $m_{\tilde{t}_1} = 800$, 442, 216, 442, 800 GeV. No (very small) stop mixing decreases Δr maximal, increases the ratio R_b maximal, etc. As a result, sfermion mixing can screen the supersymmetric radiative corrections for precision observables, even if supersymmetric particles are light $\mathcal{O}(100$ GeV).

Fig. 4 shows the Z boson observables and Δr for chargino (neutralino) masses as functions of μ for fixed $M = 100$ GeV. Stop masses are $m_{\tilde{t}_R} = 50$ GeV (solid line), 150 GeV (dotted), 800 GeV (long dotted) and $m_{\tilde{b}} = 500$ GeV without left-right mixing. $m_t = 174$ GeV and large A^0, slepton and gluino masses are assumed: $M_A = 800$ GeV, $m_{\tilde{l}} = 900$ GeV, $m_{\tilde{gl}} = 800$ GeV. In Fig. 4 $\tan\beta = 1.1$ and the experimentally excluded chargino masses are indicated by the shadowed μ range ($m_{\tilde{\chi}^\pm} \geq 48$ GeV). Close to the experimentally exluded μ region the contribution from charginos and sfermions is largest. The ratio R_b increases within the experimental 1σ range for

[a]The superscript $\Delta\rho^0$ indicates that no left-right mixing is present.

$m_{\tilde{\chi}^\pm} = 50$ GeV and $m_{\tilde{t}_R} = 50$ GeV. Larger chargino/stop masses decouple above $\mathcal{O}(500$ GeV) from the discussed observables. Larger $\tan\beta$ values give a smaller but qualitative similar result for R_b. A small value $\tan\beta = 1.1$ decreases Δr also for light $\tilde{t}_R$ masses. The ratio R_h, $\sin^2\theta_{eff}$ and the *forward-backward* asymmetry A_{FB}^b are in better agreement with the experimental data for large chargino/stop masses or strong sfermion mixing.

3.3. Upper and lower bounds at LEP I and LEP II

Fig. 5 shows the overall upper and lower bounds of the theoretical predictions for each observable individually. The results are plotted as a function of the top quark mass 130 GeV $\leq m_t \leq$ 200 GeV for the Standard Model (dashed) and the MSSM (solid). The standard Higgs mass is varied between 66 GeV $\leq M_{H_{SM}} \leq$ 800 GeV. The MSSM parameter set is restricted by the present mass bounds from direct searches at *LEP I* and $p\bar{p}$ data as shown by the solid MSSM lines in Fig. 5. Mass bounds from direct sparticle searches to be expected at *LEP II* are shown by dotted lines. An overlap between the SM and MSSM upper and lower bounds is given for large decoupled genuine supersymmetric particles and a light neutral scalar MSSM Higgs mass: $M_{h^0_{upper}} > M_{H_{SM,lower}}$. The experimental results are indicated by the dark bounds.

In case that no direct signal for supersymmetry is seen at *LEP II* , upper and lower MSSM bounds on R_b (R_c) can not explain the presently observed discrepancy with the experimental data. In conclusion from the previous results and Fig. 5 the MSSM can not improve the predictions for precision observables for light sfermions $\leq$ 300 GeV. Constraints on sfermion masses for top quark masses 160 GeV $\leq m_t \leq$ 200 GeV and $\alpha_s = 0.118...0.128$ prefer squarks $m_{\tilde{q}} > 300$ GeV, if no squark mixing is assumed. Large sfermion mixings, however, can not exclude a light stop quark $\mathcal{O}(100$ GeV).

4. Acknowledgements

We thank B. Kniehl and K. Nathan for the excellent organization during the Ringberg Workshop.

5. References

1. For a recent review see: *Precision Calculations for the Z Resonance,* Yellow report CERN 95-03, eds. D. Bardin, W. Hollik and G. Passarino, and references therein.
2. K. G. Chetyrkin, J. H. Kühn and A. Kwiatkowski, *Phys. Lett.* **B 282** (1992) 221.
   K. G. Chetyrkin and A. Kwiatkowski, *Phys. Lett.* **B 305** (1993) 285.

K. G. Chetyrkin, A. Kwiatkowski and M. Steinhauser, *Mod. Phys. Lett.* **A 29** (1993) 2785.
K. G. Chetyrkin, J. H. Kühn and A. Kwiatkowski, *Karlsruhe preprint* TTP94-10, July 1994.
3. LEP Electroweak Working Group, *CERN-preprint* LEPEWWG/95-01, March 1995.
4. F. Abe et al., *CDF Collaboration,* FERMILAB-PUB-95-022-E, March 1995.
S. Abachi et al., *DØ Collaboration,* FERMILAB-PUB-95-028-E, March 1995.
5. H. P. Nilles, *Phys. Rep.* **110** (1984) 1.
H. E. Haber and G. Kane, *Phys. Rep.* **117** (1985) 75.
J. F. Gunion and H. E. Haber, *Nucl. Phys.* **B 272** (1986) 1; *Nucl. Phys.* **B 402** (1993) 567.
J. F. Gunion, H. E. Haber, G. Kane and S. Dawson: *The Higgs Hunter's Guide,* Addison-Wesley 1990.
6. J. Ellis, S. Kelly and D. Nanopoulos, *Phys. Lett.* **B 249** (1990) 441.
U. Amaldi, W. de. Boer and H. Fürstenau, *Phys. Lett.* **B 260** (1991) 447.
P. Langacker and M. Luo, *Phys. Rev.* **D 44** (1991) 477.
7. A. Denner, R. J. Guth, W. Hollik and J. H. Kühn, *Z. Phys.* **C 51** (1991) 695.
8. F. Cornet, W. Hollik, W. Mösle, *Nucl. Phys.* **B 428** (1994) 61.
9. M. Boulware and D. Finnell, *Phys. Rev.* **D 44** (1991) 2054.
10. J. D. Wells, C. Kolda and G. L. Kane, *Phys. Lett.* **B 338** (1994) 219.
11. D. Garcia, R. A. Jiménez and J. Solà, *Barcelona preprint* UAB-FT-343, Sep. 1994; UAB-FT-344, Sep. 1994; UAB-FT-358, Jan. 1995.
12. M. Carena and C. E. M. Wagner, *CERN-preprint* CERN-TH-7393-94, Jul. 1994.
13. L. Chongsheng and H. Bingquan, *Chinese Phys. Lett.* **6** (1992) 289.
G. Bhattacharyya and A. Raychaudhuri, *Phys. Rev.* **D 47** (1993) 2014.
A. Djouadi, M. Drees and H. König, *Phys. Rev.* **D 48** (1993) 3081.
C. S. Li, B. Q. Hu, J. H. Yang and Z. Y. Fang, *J. Phys.* **G 19** (1993) 13.
L. Clavelli, *Alabama-preprint* UAHEP-948, Oct. 1994.
14. A. Dabelstein, W. Hollik, W. Mösle, in preparation.
15. A. Sirlin, *Phys. Rev.* **D 22** (1980) 971.
W. J. Marciano and A. Sirlin, *Phys. Rev.* **D 22** (1980) 2695.
16. D. Garcia and J. Solà, *Mod. Phys. Lett.* **A 9** (1994) 211.
P.H. Chankowski, A. Dabelstein, W. Hollik, W. Mösle, S. Pokorski and J. Rosiek, *Nucl. Phys.* **B 417** (1994) 101.
17. J. Fleischer, O. V. Tarasow and F. Jegerlehner, *PSI-preprint* PSI-PR-94-26, Aug. 1994.
L. Avdeev, J. Fleischer, S. Mikhailov and O. V. Tarasov, *Phys. Lett.* **B 336** (1994) 560.
J. Fleischer, O. V. Tarasov and F. Jegerlehner, *Phys. Lett.* **B 319** (1993) 249.

18. M. Böhm, W. Hollik and H. Spiesberger, *Fortschr. Phys.* **34** (1986) 687.
W. Hollik, *Fortschr. Phys.* **38** (1990) 165.
19. F. Abe et al., *CDF Collaboration,* Measurements of the W Boson Mass, FERMILAB-PUB-95/033-E and FERMILAB-PUB-95/035-E-1995.
C. K. Jung, *DØ Collaboration,* W Mass Measurements from DØ and CDF Experiments at the Tevatron, talk given at the 27th ICHEP, Glasgow, Scotland, 20-27 July 1994.
20. S. Bethke, *Proceedings of the Linear Collider Workshop,* Waikoloa 1993.
S. Catani, *Proceedings of the EPS Conference, Marseille 1993,* eds. J. Carr and M. Perrottet.
21. H. E. Haber and R. Hempfling, *Phys. Rev. Lett.* **66** (1991) 1815.
R. Hempfling and A. H. Hoang, *Phys. Lett.* **B 331** (1994) 99.
J.A. Casas, J.R. Espinosa, M. Quiros and A. Riotto, *CERN-preprint* CERN-TH. 7334/94 (July 1994).
22. J. Ellis, G. Ridolfi and F. Zwirner, *Phys. Lett.* **257 B** (1991) 83.
A. Dabelstein, *Karlsruhe preprint* KA-THEP-5-1994, to appear in Z. Phys. **C.**

6. Figure Captions

Figure 1. The observables Δr, R_b, R_c, Γ_{tot}, Γ_{ee}, $\sin^2\theta^e_{eff}$, A^b_{FB}, A^c_{FB} are plotted as a function on thepseudoscalar mass M_A for values $\tan\beta = 0.7$ (dotted line), 1.5 (long dotted), 8 (dashed-dotted), 20 (dashed) and 70 (solid). $m_t = 174$ GeV, squark and slepton masses are $m_{\tilde{q}} = 500$ GeV, $m_{\tilde{l}} = 800$ GeV, no left-right mixing. $\mu = 100$ GeV, $M = 300$ GeV and the gluino mass $m_{\tilde{gl}} = 800$ GeV.

Figure 2. The set of observables from Fig. 1. as a function on $\tan\beta$ for squark masses $m_{\tilde{b}} = 150\,(500)$ GeV and $m_{\tilde{t}_R} = 50$ GeV (solid line), 150 GeV (dotted), $300\,(500)$ GeV (long dotted, dashed), no left-right mixing. $m_t = 174$ GeV, $\mu = 100$ GeV, $M = 100$ GeV, $M_A = 800$ GeV, $m_{\tilde{l}} = 900$ GeV and $m_{\tilde{gl}} = 900$ GeV.

Figure 3. The set of observables from Fig. 1. as a function on $\tan\beta$ for stop mixing values $A_{\tilde{t}'} = -930$ GeV (dotted-dashed), -464 GeV (dashed), 0 (solid), 464 GeV (dotted), 930 GeV (long dotted). $m_{\tilde{b}} = 150$ GeV, $m_{\tilde{t}_2} = 50$ GeV and all other parameters from Fig. 2.

Figure 4. The set of observables from Fig. 1. as a function on μ for fixed $M = 100$ GeV. Stop masses are $m_{\tilde{t}_R} = 50$ GeV (solid line), 150 GeV (dotted) and 800 GeV (long dotted). $m_{\tilde{b}} = 500$ GeV, no left-right mixing, $m_t = 174$ GeV, $M_A = 800$ GeV, $m_{\tilde{l}} = 900$ GeV, $m_{\tilde{gl}} = 800$ GeV.

Figure 5. Upper and lower bounds of the individual observables as a function on m_t for the Standard Model (dashed line) and the MSSM (solid line). The MSSM parameters are restricted by the present mass bounds from direct searches at $LEPI$ and $p\bar{p}$ colliders. Mass bounds from direct sparticle searches to be expected at $LEPII$ are shown by the dotted lines.

Fig. 1

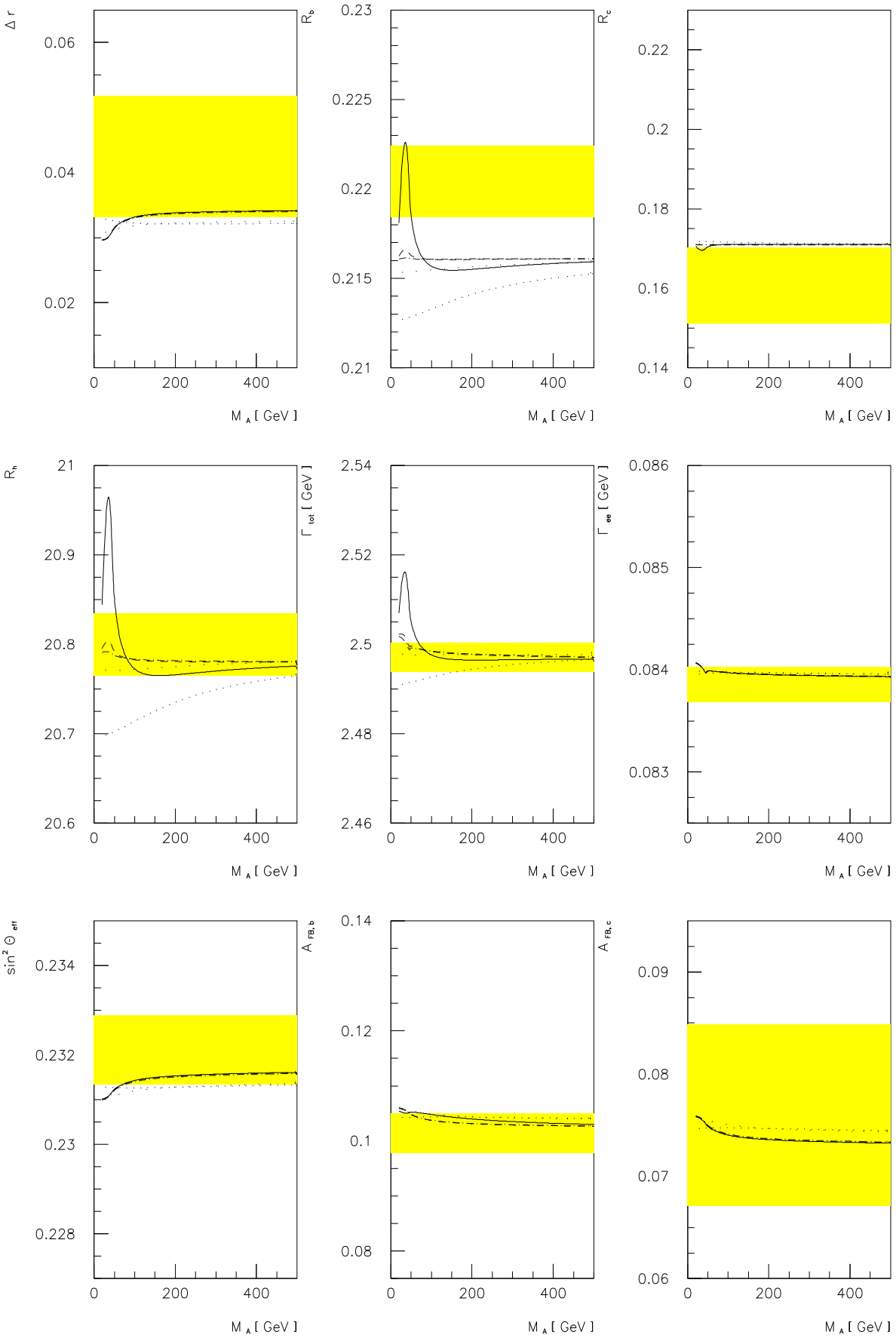
Δ r
0.06
0.04
0.02
R_b
0.23
0.225
0.22
0.215
0.21
R_c
0.22
0.2
0.18
0.16
0.14
0
200
400
M_A [GeV]
R_h
21
20.9
20.8
20.7
20.6
Γ_tot [GeV]
2.54
2.52
2.5
2.48
2.46
Γ_inv [GeV]
0.086
0.085
0.084
0.083
sin² Θ_eff
0.234
0.232
0.23
0.228
A_FB,b
0.14
0.12
0.1
0.08
A_FB,c
0.09
0.08
0.07
0.06

Fig. 2

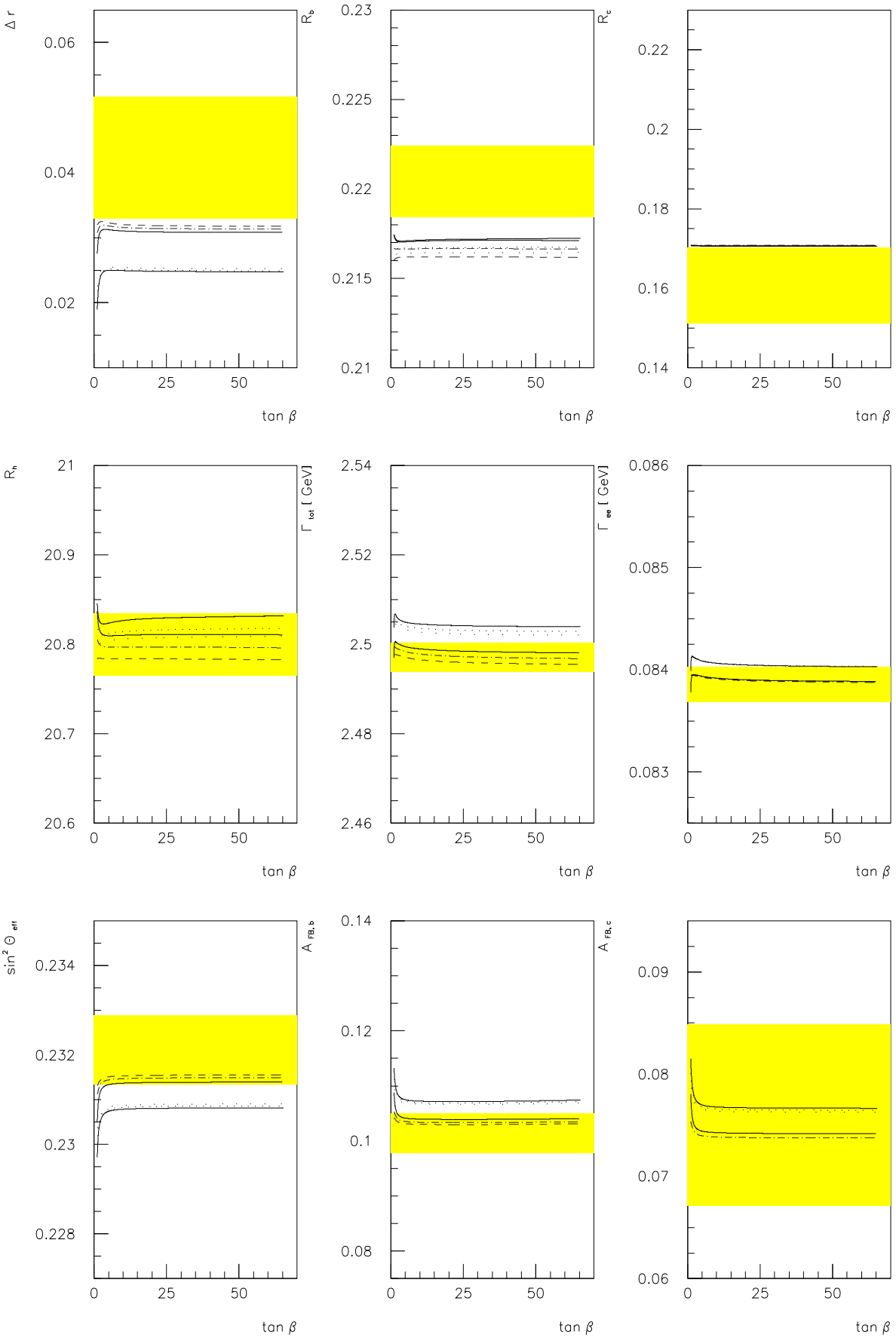
Δ r
0.06
0.04
0.02
0
25
50
tan β
R_b
0.23
0.225
0.22
0.215
0.21
R_c
0.22
0.2
0.18
0.16
0.14
R_h
21
20.9
20.8
20.7
20.6
Γ_tot [GeV]
2.54
2.52
2.5
2.48
2.46
Γ_inv [GeV]
0.086
0.085
0.084
0.083
sin² Θ_eff
0.234
0.232
0.23
0.228
A_FB,b
0.14
0.12
0.1
0.08
A_FB,c
0.09
0.08
0.07
0.06

Fig. 3

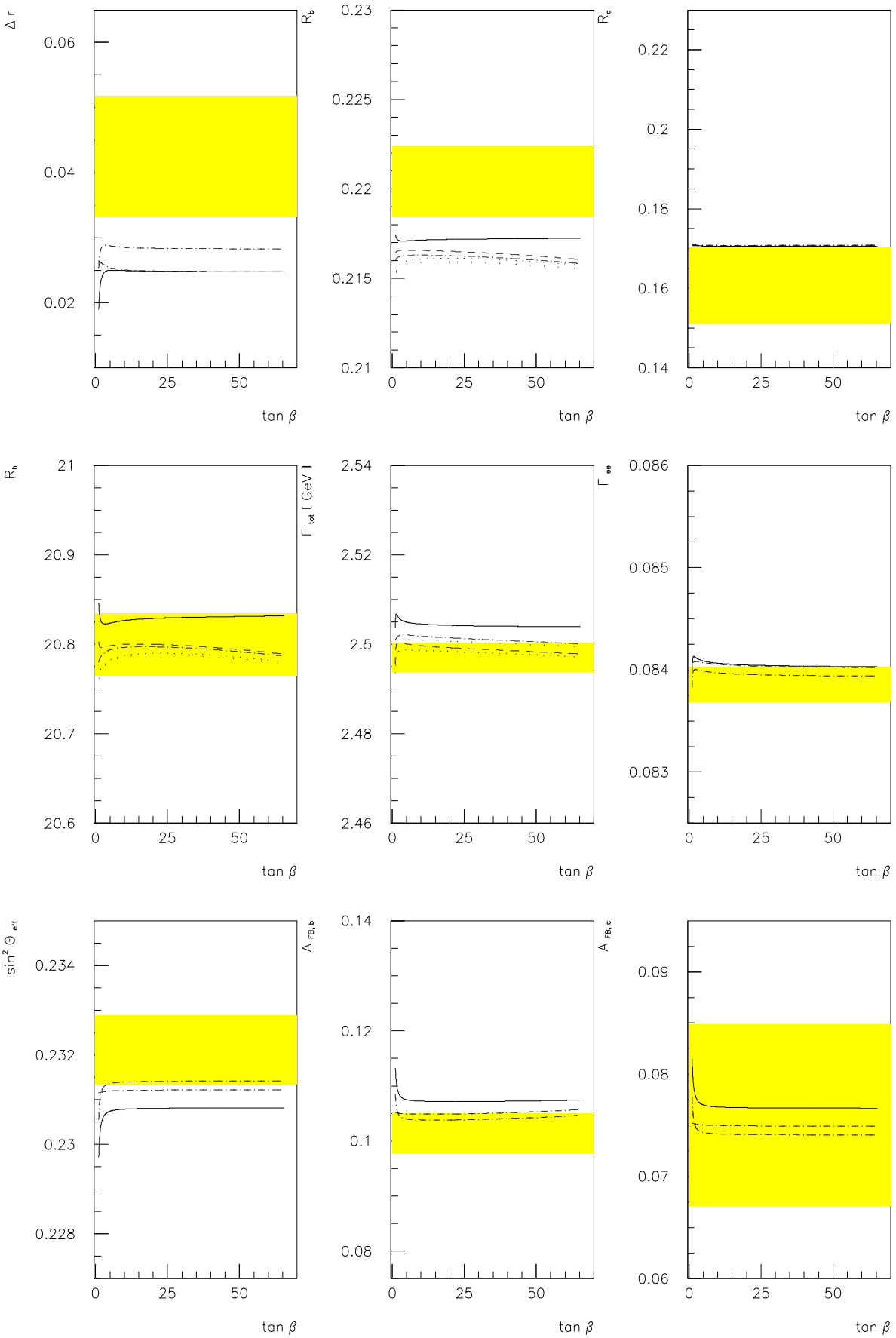
Δ r
0.06
0.04
0.02
0
25
50
tan β
R_b
0.23
0.225
0.22
0.215
0.21
R_c
0.22
0.2
0.18
0.16
0.14
R_h
21
20.9
20.8
20.7
20.6
Γ_tot [GeV]
2.54
2.52
2.5
2.48
2.46
Γ_ee
0.086
0.085
0.084
0.083
sin² Θ_eff
0.234
0.232
0.23
0.228
A_FB,b
0.14
0.12
0.1
0.08
A_FB,c
0.09
0.08
0.07
0.06

Fig. 4

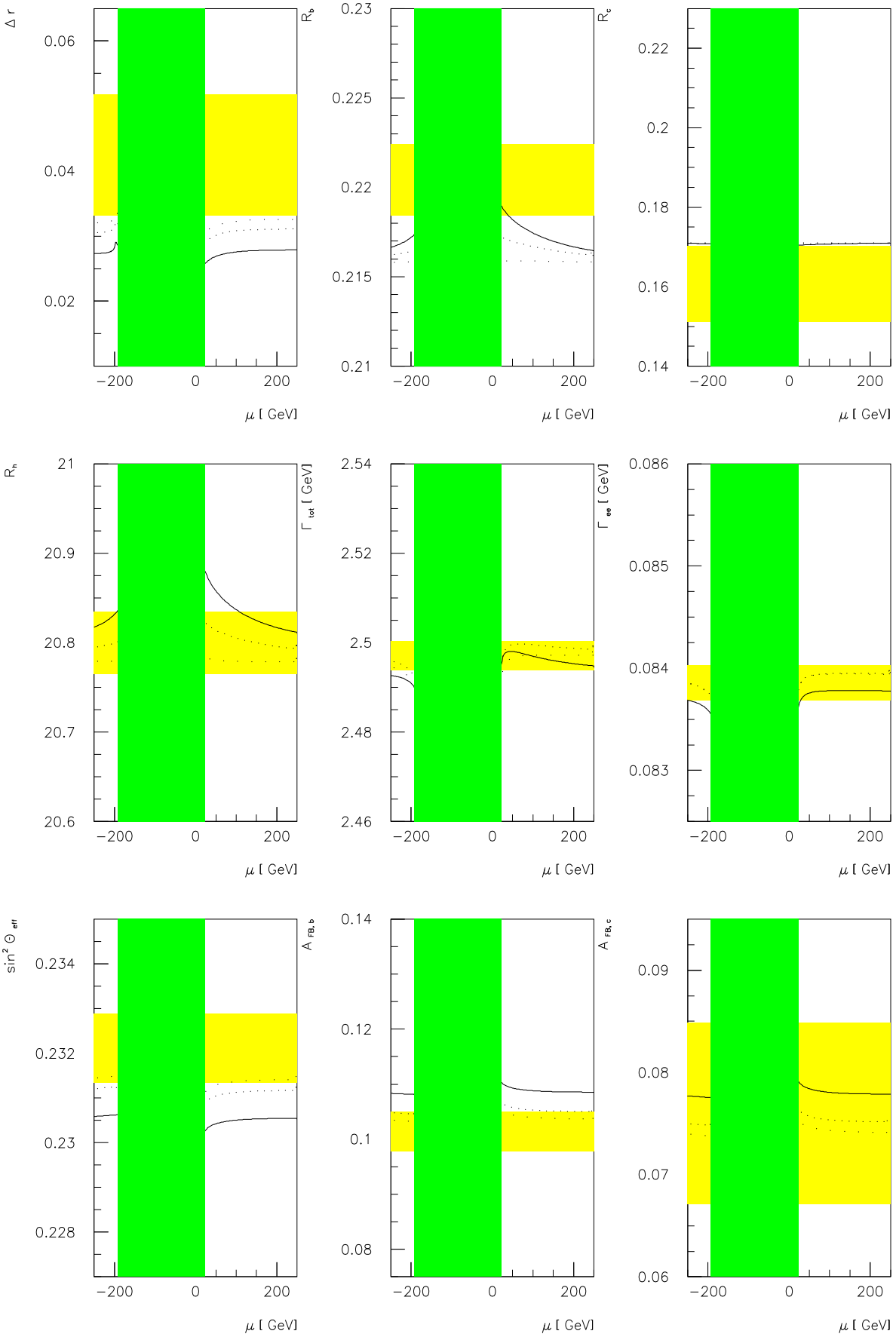
Δ r
0.06
0.04
0.02
−200
0
200
μ [GeV]
R_b
0.23
0.225
0.22
0.215
0.21
R_c
0.22
0.2
0.18
0.16
0.14
R_h
21
20.9
20.8
20.7
20.6
Γ_tot [GeV]
2.54
2.52
2.5
2.48
2.46
Γ_had [GeV]
0.086
0.085
0.084
0.083
sin² Θ_eff
0.234
0.232
0.23
0.228
A_FB,b
0.14
0.12
0.1
0.08
A_FB,c
0.09
0.08
0.07
0.06

Fig. 5

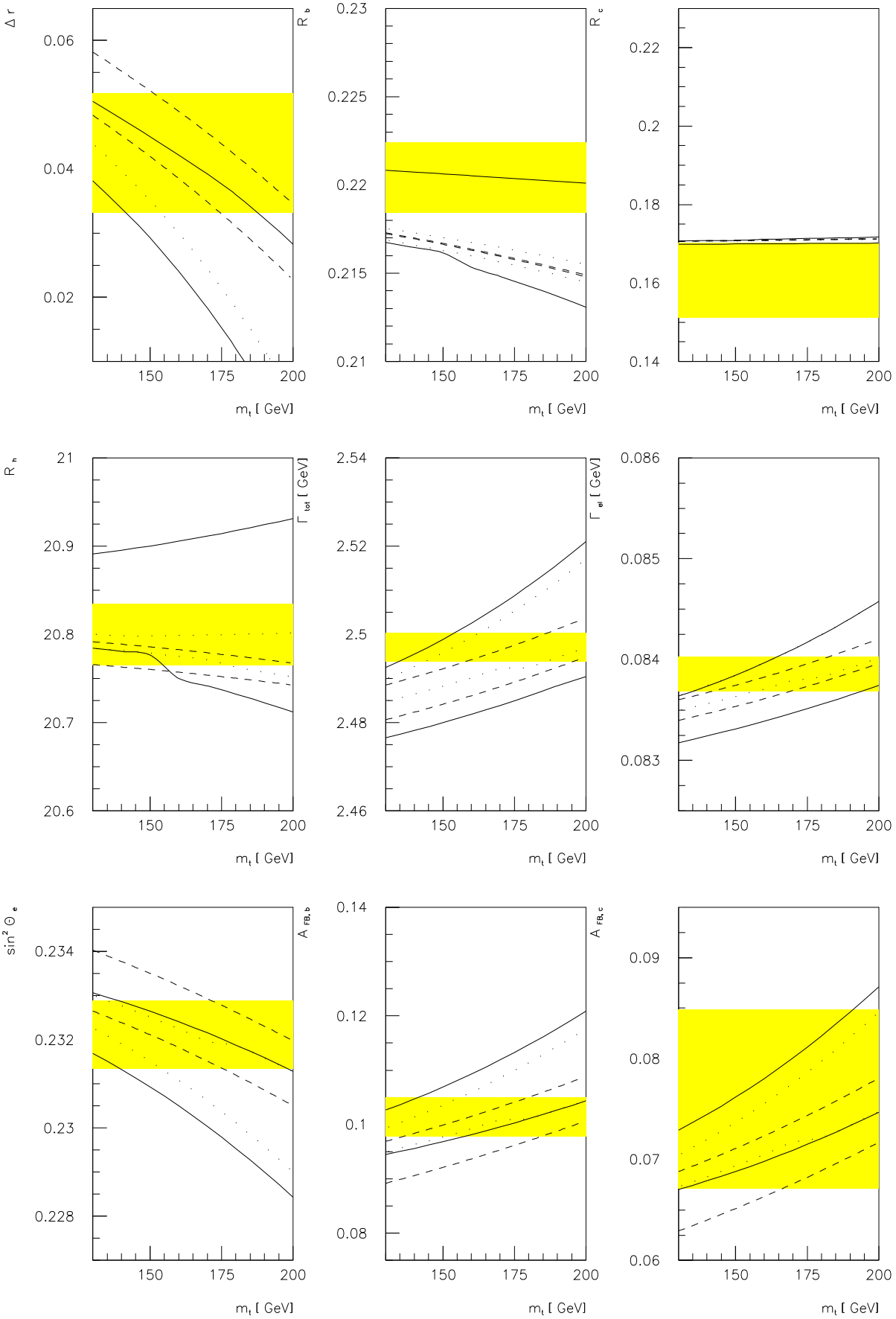
Δ r
0.06
0.04
0.02
150
175
200
m_t [GeV]
R_b
0.23
0.225
0.22
0.215
0.21
R_c
0.22
0.2
0.18
0.16
0.14
R_h
21
20.9
20.8
20.7
20.6
Γ_tot [GeV]
2.54
2.52
2.5
2.48
2.46
Γ_el [GeV]
0.086
0.085
0.084
0.083
sin² Θ_e
0.234
0.232
0.23
0.228
A_FB,b
0.14
0.12
0.1
0.08
A_FB,c
0.09
0.08
0.07
0.06